Baker IDI
HEART & DIABETES INSTITUTE

Baker IDI Research Online
http://library.bakeridi.edu.au

This is the postprint version of the work. It is the manuscript that was accepted by the journal following peer review. It does not include the publisher's layout and pagination.

Ardipradja K, Yeoh SD, Alt K, O'Keefe G, Rigopoulos A, Howells DW, Scott AM, Peter K, Ackerman U, Hagemeyer CE. Detection of activated platelets in a mouse model of carotid artery thrombosis with 18 F-labeled single-chain antibodies. Nucl Med Biol 2014;41(3):229-37.

http://hdl.handle.net/11187/1995

Copyright © Elsevier. This file is for personal use. Further distribution is not permitted.

*Manuscript
Click here to view linked References

Detection of activated platelets in a mouse model of carotid artery thrombosis with ^{18}F-labeled single-chain antibodies

Katie Ardipradja[1,2,3,4], Shinn Dee Yeoh[3], Karen Alt[1,2], Graeme O'Keefe[3], Angela Rigopoulos[5], David W. Howells[6], Andrew M. Scott[3,4,5], Karlheinz Peter[2,7,*], Uwe Ackerman[3,4,5,*], Christoph E. Hagemeyer[1,7,*#]

[1] Vascular Biotechnology Laboratory, Baker IDI, Melbourne, Australia

[2] Atherothrombosis and Vascular Biology Laboratory, Baker IDI, Melbourne, Australia

[3] Departments of Nuclear Medicine and Centre for PET, Austin Hospital, Melbourne, Australia

[4] Department of Medicine, Dentistry and Health Sciences, The University of Melbourne, Melbourne, Australia

[5] Ludwig Institute for Cancer Research, Austin Hospital, Melbourne, Australia

[6] The Florey Institute of Neuroscience and Mental Health, Austin Hospital, Melbourne, Australia

[7] Central Clinical School, Monash University, Melbourne, Australia

*Equally contributing senior authors

Keywords: antibodies, thrombosis, platelets, PET/CT

#Corresponding author: CE Hagemeyer, Vascular Biotechnology Laboratory,

Baker IDI Heart and Diabetes Institute, 75 Commercial Road, Melbourne Victoria 3004, Australia, Phone: +61 3 8532 1494; Fax: +61 3 8532 1100

e-mail: christoph.hagemeyer@bakeridi.edu.au

Abstract

Introduction: Activated platelets are key players in thrombosis and inflammation. We previously generated single-chain antibodies (scFv) against ligand-induced binding sites (LIBS) on the highly abundant platelet glycoprotein integrin receptor IIb/IIIa. The aim of this study was the construction and characterisation of a novel ^{18}F PET radiotracer based on this antibody.

Methods: ScFv$_{anti\text{-}LIBS}$ and control antibody mut-scFv were reacted with N-succinimidyl-4-[^{18}F]fluorobenzoate (S[^{18}F]FB). Radiolabeled scFv was incubated with *in vitro* formed platelet clots and injected into mice with $FeCl_3$ induced thrombus in the left carotid artery. Clots were imaged in the PET scanner and amount of radioactivity measured using an ionization chamber and image analysis. Assessment of vessel injury as well as the biodistribution of the radiolabeled scFv was studied.

Results: After incubation with increasing concentrations of ^{18}F-scFv$_{anti\text{-}LIBS}$ clots had retained significantly higher amounts of radioactivity compared to clots incubated with radiolabeled ^{18}F-mut-scFv (13.3 ± 3.8 vs 3.6 ± 1 KBq, $p < 0.05$, $n = 9$, decay corrected). In the *in vivo* experiments we found an high uptake of the tracer in the injured vessel compared with the non-injured vessel, with 12.6 ± 4.7% injected dose per gram (ID/g) uptake in the injured vessel and 3.7 ± 0.9% ID/g in the non-injured vessel 5 minutes after injection ($p < 0.05$, $n=6$).

Conclusions: Our results show that the novel antibody radiotracer ^{18}F-scFv$_{anti\text{-}LIBS}$ is useful for the sensitive detection of activated platelets and thrombosis.

Advances in knowledge and implications for patient care: We describe the first ^{18}F variant of a scFv$_{anti\text{-}LIBS}$ against activated platelets. This diagnostic agent could provide a powerful tool for the assessment of acute thrombosis and inflammation in patients in the future.

Introduction

Mortality from acute thrombosis such as myocardial infarction and stroke caused by rupture of atherosclerotic plaques remains high due to limitations in our ability to diagnose vulnerable rupture prone plaques that cause little or no stenosis [1]. Currently, diagnosis by coronary angiography in patients presenting with angina pectoris provides information about the vessel lumen but not the morphology of the vessel wall itself, which is critical to distinguish unstable, rupture-prone plaques from stable plaques [2]. Platelets play a key role in atherosclerosis and atherothrombosis [3]. They can be found on the surface of inflamed non-ruptured vulnerable plaques [4-6], and after plaque rupture they participate in thrombus formation [3,7].

Early and non-invasive detection of platelets associated with vulnerable plaques would be of clinical interest before total thrombotic occlusion of vessels occurs. Molecular imaging of cells or cellular epitopes is a rapidly evolving field, which allows non-invasive detection of certain pathologies [8,9]. Targeting surface epitopes in atherosclerosis has been described in various animal models, allowing detection of early atherosclerosis or thrombus formation in arterial vessels [10,11].

Molecular imaging has most commonly utilized monoclonal antibodies to detect molecular targets associated with disease, however due to their relatively large size radiolabeled monoclonal antibodies persist in the circulation for an extended period of time of days to weeks [12]. This persistence is not ideal for PET imaging especially with short lived radio-isotopes such as ^{18}F as it causes a high background signal making targeted uptake difficult to distinguish. Ideally smaller antibody fragments lacking the Fc portion should be used for PET imaging, as antibody fragments lacking the Fc portion are cleared more rapidly [13]. ScFvs consist of the variable light and variable heavy portions of an antibody and are ideal for

imaging as they are cleared rapidly from the circulation and are able to penetrate tissues [14,15].

Molecular imaging of activated platelets on the surface of arterial thrombosis has been described previously with magnetic resonance imaging (MRI) [6,16,17]. Microparticles of iron oxide (MPIO) were conjugated to a scFv targeted to the ligand–induced binding site of the activated glycoprotein IIb/IIIa-receptor. These microparticles typically cause a signal void in T2*-weighted MRI. These targeted MPIO's allowed the non-invasive detection of a non-occlusive, wall-adherent thrombus in the carotid arteries of mice *in vivo*. Monitoring thrombus size and thrombolytic therapy was made possible using these microparticles [6]. However due to the negative contrast created by iron oxide based contrast reagents, the obtained signal can often be disturbed by motion artefacts [18,19]. The lack of sensitivity of these microparticles may also make them ineffective at detecting small platelet aggregates that are typically associated with inflammatory development of vulnerable atherosclerotic plaques. Therefore improving the sensitivity and decreasing the problems associated with motion artifacts is important, especially in the context of detecting coronary plaques where motion artifacts are significant due to the constant movement of the heart. Radiotracers provide excellent sensitivity allowing detection in the picomolar range [20,21]. Radiotracer sensitivity of detection is also less affected by motion artifacts in comparison to MRI contrast reagents [19]. We have previously investigated imaging of activated platelets in SPECT [22]. Given the even higher sensitivity of PET over SPECT, the aim of this study was the construction and characterization of a novel radiotracer for use in PET targeting the LIBS epitope of activated platelets. We used a well described non-blocking scFv against GPIIbIIIa on activated platelets as well as a non-binding control scFv [6,17,23-25]. We used both *in vitro* formed human clots rich in activated platelets as well as an *in vivo* mouse model of a

wall adherent non-occlusive thrombosis. Firstly, $scFv_{anti\text{-}LIBS}$ was conjugated to Succinimidyl-4-^{18}F-fluorobenzoate. Then, binding of the radiotracer to activated platelets was tested by flow cytometry and autoradiography. In the *in vivo* model, the thrombus was detected using PET. This approach allowed the accurate and highly sensitive detection of activated platelets in the vessel. This radiotracer is hoped to be applicable to the future detection of activated platelets associated with atherosclerosis and atherothrombosis in humans.

Material and methods

Production of $scFv_{anti\text{-}LIBS}$

$ScFv_{anti\text{-}LIBS}$ and mut-scFv were produced in an *E.coli* expression system. Characterization and purification of scFv have been described previously [23,26]. In brief: the scFv was produced in TG1 *E.coli* transformed with a pHOG expression vector containing the sequence for the scFv with a histidine protein purification tag. Bacterial pellets were collected from 1 litre cultures that were allowed to grow for 5 hours at 37° C. A lysate was produced using a protein extraction buffer according to the manufacturer's instruction (BugBuster, Merck/ Novagen). The lysate was cleared and his-tagged antibodies were extracted from the cleared lysate on a FPLC system with 5 ml columns packed with Ni-agarose beads (Ni-NTA Superflow cartridge, Qiagen,). The captured scFv was eluted from the column with 250 mM imidazole, fractions containing high levels of protein were dialysed against PBS (pH 7.2) to remove excess imidazole from the pure scFv solution. Samples of fractions from the purification were analyzed by SDS-PAGE under reducing conditions. The binding function of the purified antibody was evaluated using flow cytometry. Protein concentration was determined using BCA protein assay (Pierce, Thermo Scientific).

Radiolabeling

500 µg of purified ScFv in 500 µl PBS (with Ca^{2+}/Mg^{2+}) was added to dried N-Succinimidyl-4-^{18}F-fluorobenzoate (^{18}F-SFB) which was synthesized as described previously in full lead shielding [27]. The reaction was gently mixed on a rotor for 30 minutes at room temperature. Free ^{18}F-SFB was removed from the radiolabeled scFv using 10 KD cut-off 0.5 ml centrifugal filters (Amicon Ultra, Millipore). Reactions were spun in a bench-top centrifuge for 20 minutes at 16,000 x *g* and washed twice with PBS to remove excess ^{18}F-SFB. The radioactivity of labeled scFv was measured using a CRC-25W well counter (Capintec Inc, New Jersey, USA). The function of the radiolabeled scFv was tested using flow cytometry after full decay as described before [23,26]. In short, platelet rich plasma was collected from the blood of healthy volunteers. Non-activated and activated platelets (stimulated with adenosine diphosphate, ADP, Sigma) were incubated with radiolabeled $scFv_{anti\text{-}LIBS}$ / control scFv, and following this, platelets were incubated with a secondary antibody conjugated to a fluorochrome (Penta HIS Alexa Fluor 488, Qiagen) which selectively binds to the histidine-protein-purification-tag. Platelets were fixed and analyzed on a BD FACScalibur flow cytometer, fluorescence signal was examined on 10,000 gated events. Assessment of fluorescence signal was conducted using CellQuest Pro software.

***In vitro* platelet rich clots**

In vitro formed platelet rich clots were used to evaluate binding of labeled scFv as described before [28]. In summary, platelet rich plasma was collected from the blood of healthy volunteers. 0.5 ml of plasma was added to 50 µl of ADP (200 µMol/ml), 44 µl Actin FS, (Dade Behring, Siemens diagnostics) 12.5 µl $CaCl_2$ (1 M) in a 1.5 ml tube. The mixture was then incubated at 37° C for 12 minutes until a solid clot formed. Solid clots were washed in

PBS (with Ca^{2+}/Mg^{2+}) prior to incubation with radiolabeled scFv (15 minutes at room temperature). After incubation radioactivity retained by the clots was measured using an ionization chamber and a PET scan of the clots were obtained using a Philips Allegretto PET scanner. Experiments to demonstrate specificity of binding were also performed. After washing in PBS a group of clots were pre-incubated with increasing amounts of cold non-labeled $scFv_{anti\text{-}LIBS}$ for 30 minutes at room temperature prior to incubation with ^{18}F-$scFv_{anti\text{-}LIBS}$. Radioactivity retained was compared to clots only incubated with radiolabeled $scFv\text{-}_{anti\text{-}LIBS}$ alone. Absolute amounts of scFv incubated with the clots were determined after the incubation experiment and once the radioactivity had decayed using BCA protein assay. The amount of scFv in microgram varies from 71.19 ± 14.34 µg, 124.54 ± 21.96 µg, 276.11 ± 45.25 µg ($scFv_{anti\text{-}LIBS}$) to 161.66 ± 47.86 µg, 200.82 ± 35.06 µg, 381.47 ± 66.16 µg (mut-scFv) for 10 µl, 20 µl and 40 µl respectively. After both these processes clots were embedded and frozen in OCT for histological analysis.

Acute carotid artery thrombosis model

An established carotid artery thrombosis model in mice was used to induce a small wall adherent thrombus [6,24]. In brief, 12-16 weeks old female C57BL/6 mice weighing > 22g were anesthetized by intraperitoneal injection of ketamine (100µg/kg body weight, BW) and xylazine (5 µg/kg BW) and were then placed under a dissecting microscope. Under full anesthesia a segment of the left carotid artery of the mouse was isolated by a superficial incision of the skin and blunt dissection of the fascia surrounding the vessel. This vessel was exposed to a 3x3 mm filter paper impregnated with a 5% $FeCl_3$ solution for 3 minutes, after which the filter paper was removed and the wound sealed with surgical tape, mice were then kept on a 37º C heating-pad and full anesthesia maintained. A wall-adherent thrombus was

allowed to develop for 25min. The right carotid artery was left untouched as the control non-injured vessel. Following this, 100 µl of radiolabeled scFv was injected via the tail vein. Mice were then used in biodistribution experiments or PET imaging.

Biodistribution studies

After the induction of an acute thrombus mice were each injected via the tail vein with radiolabeled $scFv_{anti\text{-}LIBS}$ (953.52 ± 211.05 µg) or radiolabeled mut-scFv (877.60 ± 225.82 µg) in 100 µl PBS (with Ca^{2+}/Mg^{2+}). The mice were killed and dissected at 5, 15, 30, and 45 minutes after injection. The blood, major organs and both carotid arteries were collected and the wet weight and radioactivity of all tissues were measured were counted on a Wallac WIZARD Automatic Gamma Counter (Perkin Elmer Inc). The results are presented as percentage injected dose per gram (%ID/g). The radioactivity in the tissue samples for each mouse was standardised against a known amount of the injected dose. Afterwards the injured and contralateral vessels were embedded in OCT TissueTec (Sakura Finetec, Japan), sectioned and immuno-stained as described before [6]. In addition one group of mice were pre-injected with increasing concentrations of non-labeled $scFv_{anti\text{-}LIBS}$ 30 minutes prior to injection of ^{18}F-$scFv_{anti\text{-}LIBS}$. Organs and carotid arteries were collected and radioactivity was measured as described earlier.

Small animal imaging

Prior to the PET scan, a whole body CT image was obtained on Philips Gemini PET/CT hybrid system (90 kVp, 100 mAs, 50 mm transaxial FOV) which was reconstructed to an image with a voxel size of 0.098×0.098×1.000 mm. After thrombus induction and injection of radiolabeled scFvs, 1 hour dynamic PET images were obtained on Philips Allegretto PET

scanner in 5 minute frames. Both PET and CT images were imported into the Fusion toolbox of PMOD 3.2 (PMOD technologies Ltd., Zürich, Switzerland) for spatial co-registration and subsequent image analysis.

ROI's were drawn in the CT image for both injured vessel and intact vessel. From the ROI a VOI was generated. A VOI with the same volume as the injured vessel VOI was also generated for skeletal muscle on the right hindlimb of each mouse and radioactivity uptakes were examined. Counts per voxel for each VOI were determined and ratios between the injured vessel and skeletal muscle as well as intact vessel and skeletal muscle was determined. After gamma counting both carotid arteries were embedded in OCT TissueTec and sectioned as described in the previous section.

Statistical analysis

Data was subjected to 2 tailed student t-test. All presented quantitative data were expressed as mean ± SEM. Means were compared by use of a 1-way ANOVA and the Student t-test. P values of less than 0.05 were considered statistically significant. Number of animal are indicated in the results section and figure legends.

Ethics statement

Care and use of laboratory animals followed the national guidelines and was approved by the institutional animal ethics committees of the University of Melbourne, Austin Hospital Heidelberg.

Results

ScFv$_{anti\text{-}LIBS}$ production and purification

Expression of scFv$_{anti\text{-}LIBS}$ in BL21 *E.coli* cultures yielded 10 µg/ml of culture and for mut-scFv cultures 9 µg/ml. After affinity chromatography, purified proteins were analyzed by SDS-PAGE. On the SDS gel the scFv migrated as monomers at the predicted molecular mass of 33 kDa under reducing conditions (data not shown).

Radiolabeling and immunoreactivity

The synthesis of ^{18}F-SFB was conducted in a fully automated synthesis module according to a methods reported recently by us [29] with typical decay corrected radiochemical yields of around 80%. The specific activity of ^{18}F-SFB was 80–149 GBq/µmol at the end of synthesis as determined by radio HPLC and radiochemical purity was determined to be 97%. ScFv$_{anti\text{-}LIBS}$ and mut-scFv were added to dried ^{18}F-SFB and the conjugation was performed for 30 minutes. The specific activity of ^{18}F-scFv$_{anti\text{-}LIBS}$ and ^{18}F-mut-scFv was 405 ± 141 MBq/mmol and 521 ± 111 MBq/mmol respectively. After conjugation and to obtain the final formulation the labeled scFv was purified from free ^{18}F-SFB. The radiotracer showed negligible amounts of free SFB left after two washes with less than 0.5% of the initial ^{18}F-SFB amount remaining in the second wash fraction. The radiochemical yield for ^{18}F-scFv$_{anti\text{-}LIBS}$ and ^{18}F-mut-scFv was 1.8 ± 0.5% and 3.2 ± 0.6% respectively.

Binding activity of the radiolabeled scFv$_{anti\text{-}LIBS}$ to activated platelets in flow cytometry was decreased compared to non-labeled scFv$_{anti\text{-}LIBS}$ (n=7, p=0.025). Platelets incubated with 1 µg of ^{18}F-scFv$_{anti\text{-}LIBS}$ showed 34.4 ± 11.4% positive staining in comparison to non-labeled scFv$_{anti\text{-}LIBS}$ with 61.1 ± 13.1% of platelets positive (Fig. 1A). ^{18}F-scFv$_{anti\text{-}LIBS}$ showed minimal non-specific binding to non-activated platelets and this was not significantly

different from non-labeled $scFv_{anti\text{-}LIBS}$. ^{18}F-mut-scFv showed no binding to platelets in the radiolabeled or non-labeled form (Fig. 1B).

Clot binding assay

In vitro formed clots incubated with increasing amounts of labeled scFv retained a significantly greater amount of activity in comparison to clots that were incubated with ^{18}F-mut-scFv ($p<0.01$). Clots incubated with ^{18}F-$scFv_{anti\text{-}LIBS}$ retained 3.4 ± 0.1% of the original activity in comparison to clots incubated with ^{18}F-mut-scFv which only retained 1.3 ± 0.1% of the original activity (Fig. 2A). Clots incubated with ^{18}F-$scFv_{anti\text{-}LIBS}$ showed significantly higher counts per voxel in comparison to clots that were incubated with ^{18}F-mut-scFv. Immunohistochemistry of these clots are also positive for the platelet marker CD41, confirming the presence of the target receptor on platelets (Fig. 2B). Clots that were pre-incubated with non-labeled $scFv_{anti\text{-}LIBS}$ showed significantly lower radioactivity uptake in comparison to clots incubated with ^{18}F-$scFv_{anti\text{-}LIBS}$ alone (Fig. 2C).

Biodistribution

Biodistribution of ^{18}F-$scFv_{anti\text{-}LIBS}$ was conducted in female C57/BL6 mice with a thrombus induced only in the left carotid artery by $FeCl_3$ injury. As seen in Fig. 3A ^{18}F-$scFv_{anti\text{-}LIBS}$ is excreted rapidly via the renal pathway with the accumulation of activity in the kidney rising sharply 5 minutes (21.3 ± 9.5% ID/g) and 15 minutes (24.8 ± 13.8% ID/g) after injection. Due to excretion into the bladder the accumulated activity in the kidney decreases beyond 15 minutes. Uptake in all organs including the injured vessel is high at 5 minutes after injection and the only organ with a higher uptake than the injured vessel is the kidney. The activity in the blood pool was low (10.5 ± 4.4% ID/g) and also decreased over all time points

investigated. Activity accumulation in the injured vessel was significantly higher in comparison to the intact vessel at 5 minutes (12.6 ± 4.7% ID/g compared to 3.7 ± 0.9% ID/g). The uptake of ^{18}F-scFv$_{anti\text{-}LIBS}$ decreased in all organs over time. Despite this, the ratio of uptake in the injured vessel compared to blood remained steady between 15-45 minutes after injection. Ratio of uptake in the injured vessel : muscle between 5 and 45 minutes after injection was also high (164.8 ± 76.9, 49.6 ± 11.2, 73.4 ± 25.8, 44.3 ± 12.7 at 5, 15, 30 and 45 minutes after injection). The radiolabeled mut-scFv showed no significant difference in uptake between the injured and intact vessel ($p>0.05$) at all time points investigated. Pre-injection of scFv$_{anti\text{-}LIBS}$ of all concentrations inhibited ^{18}F-scFv$_{anti\text{-}LIBS}$ uptake in the injured vessel (Fig. 3B) in comparison to mice injected with ^{18}F-scFv$_{anti\text{-}LIBS}$ alone (100 µg, 200 µg, pre-injection uptake: 3.6 ± 1.5% ID/g, 2.3 ± 0.7% ID/g, uptake of control, ^{18}F-scFv$_{anti\text{-}LIBS}$ alone: 13.4 ± 4.7% ID/g).

PET imaging and histology

High contrast PET images of the whole body were acquired at 45 minutes after injection. Coronal, sagital and axial images from 45 minutes after injection are shown in Fig. 4A. Specific tracer accumulation is observed in the injured vessel compared to the non-injured vessel (arrow in Fig. 4A). We also observed high uptake of both the mut-scFv and scFv$_{anti\text{-}LIBS}$ radiotracers in the kidney and bladder which correlated well to the biodistribution study and supports a renal clearance pathway for the scFv radiotracers. Injured and intact vessels were collected for immunohistochemistry after biodistribution and scanning and were stained with anti-CD41 to confirm the presence of platelets in the injured vessel. Immunohistochemistry on the resected carotid vessels revealed positive staining for the platelet marker CD41 in vessels that were exposed to the ferric chloride solution confirming

the presence of platelets in those sections. In contrast, immunohistochemistry on intact vessel sections showed no CD41 staining. These results indicate that the intact vessel was suitable as a platelet negative control (Fig. 4B).

PET image analysis

VOI analysis reveals that ^{18}F-scFv$_{anti\text{-}LIBS}$ began to accumulate 5 minutes after injection. ^{18}F-scFv$_{anti\text{-}LIBS}$ uptake in the injured vessel was significantly higher than the uptake in the intact vessels after injection when normalized to uptake in muscle, chosen as a background tissue (Fig. 5A, ratio of counts/voxel of injured vessel to skeletal muscle: 2.8 ± 0.6; ratio of counts/voxel of intact vessel to skeletal muscle: 1.6 ± 0.4, n=8, $p<0.05$). Analysis of uptake of ^{18}F-mut-scFv revealed no significant difference between injured and non-injured vessels over the 1 hour scan. The average ratio of radioactivity uptake of injured : intact vessels were 2.4 ± 0.2 for ^{18}F-scFv$_{anti\text{-}LIBS}$ and 1 ± 0.1 for ^{18}F-mut-scFv (Fig. 5B). In contrast to the biodistribution analysis where the optimal time point was at 5min, for the imaging results we conclude that 45minutes after injection appears to be the optimal time point to obtain a high contrast image as the activity in the blood pool and non-associated organs has largely been cleared. The region of skeletal muscle used for the analysis is shown in Fig. 5C.

Discussion

In this study, we developed a novel immunoPET radiotracer capable of targeting the GPIIb/IIIa surface antigen in its active conformation. The activated receptor is essential for mediating platelet aggregation and is expressed in abundant quantities on the surface of activated platelets [30,31] which are a major component of thrombi. Human platelets express between 30-100,000 GPIIb/IIIa receptors on their surface [30]. Murine platelets have

comparable expression with a reported 60-80,000 receptors per platelets [32]. The estimated number of LIBS sites in the *in vitro* formed clots are estimated to be 6.5 x 10^{12} based on the assumption that 1 µl of PRP contains 200,000 platelets [33] and each platelet carries on average 65,000 receptors. Accordingly i*n vivo,* with an approximate thrombus volume of 2.4 µl, the estimated number of LIBS in the thrombus is 3 x 10^{10}. The actual accessible target density *in vivo* and *in vitro* will be smaller because not all receptors are exposed to the antibody.

The abundance and association of this antigen with activated platelets makes it an ideal target for molecular imaging of thrombi. We have previously generated scFv which targets the GPIIb/IIIa in it's active conformation as well as a control non-binding mut-scFv [23,26]. Despite having slightly lowered immunoreactivity after radiolabeling with ^{18}F-SFB (56% of unlabeled scFv binding) the targeted scFv was still able to accumulate in the target thrombi, both in *in vitro* formed human clots as well as the *in vivo* thrombi generated in mouse model of acute thrombosis induced by exposure to $FeCl_3$. This indicates that good binding affinity, and retention of specificity was still present after radiolabeling. Previous studies using ^{18}F-SFB to radiolabel small antibody fragments also showed decreased immunoreactivity after radiolabeling [34]. The lowered immunoreactivity could be attributable to the presence of lysine residues in the antigen binding site of the scFv. A site specific method of radiolabeling may improve radiolabeling positron emitting isotopes to these antibodies without compromising their binding activity.

Nevertheless in our study the radiolabeled scFv shows specific GPIIb/IIIa targeting with high contrast images generated at 45-50 minutes post injection. Pre-incubation of *in vitro* formed clots with non-labeled $scFv_{anti\text{-}LIBS}$ reduces radioactivity uptake in comparison to clots incubated with ^{18}F-$scFv_{anti\text{-}LIBS}$ alone. Non-labeled $scFv_{anti\text{-}LIBS}$ was also pre-injected *in vivo*

and at 5 minutes after injection these pre-injected mice had no significant difference in radioactivity uptake between the injured and intact vessels. This demonstrates that uptake of ^{18}F-scFv$_{anti\text{-}LIBS}$ can be specifically blocked. Due to the relatively small size of the scFv and the absence of the Fc portion in this antibody format, clearance was expected to be quite rapid via the renal pathway. There is little accumulation in other organs such as spleen, liver, heart or lung. This is in line with previous reports using even smaller RGD peptides as radio-tracers to detect integrins [35]. Primarily designed to detect the αvβ3 integrin during cancer angiogenesis on inflamed endothelia cells, it is also expressed by macrophages in atherosclerotic lesions [36]. Furthermore, RGD peptides are cross-reactive to the GPIIbIIIa integrin and can be used to detect platelets. However, in contrast to our scFv$_{anti\text{-}LIBS}$, RGD peptides are ligand mimetics and can cause activation of platelets [37,38] and may therefore not be suitable for diagnostic imaging in patients. Our biodistribution results showed gradually increasing radioactivity at later time points in the kidneys for both scFv's demonstrating renal clearance of the scFv. The fast clearing of the scFv is ideal for imaging in the setting of acute thrombosis where the window for obtaining images is relatively brief. We typically see thrombus formation in our model after 3-5 mins, which reflects acute thrombotic events in humans following plaque rupture leading to myocardial infarction and stroke. A larger antibody format, such as a whole IgG, would be unsuitable due to it's longer serum half-life of up to 110 hours in comparison to scFv's which generally have a serum half-life of about 2 hours [14]. The presence of the Fc portion on IgG's also adds to it's prolonged serum half-life as it reacts with neonatal Fc receptors (FcRn). An undesirable potential side effect of the Fc portion is the inappropriate activation of cells expressing Fc receptors which can cause cytotoxic effects [39]. Prolonged serum half-life of radiolabeled antibodies also means prolonged radiation exposure for other non-target tissues which is also undesirable.

The choice of ^{18}F as the radiolabel instead of positron emitter with a longer half-life was also considered and the broad availability of ^{18}F and its radioactive half-life being suitably matched to the serum half-life of scFv, made it the isotope of choice.

Specific activity of ^{18}F-$scFv_{anti\text{-}LIBS}$ is relatively low at 405 ± 141 MBq/mmol after purification and separation from free ^{18}F-SFB. This is at the lower end of what is regarded as optimal for human use. Use of ^{18}F-SFB as a method for radiolabeling small recombinant antibodies such as $scFv_{anti\text{-}LIBS}$ is always a trade off between specific activity and antibody binding. The specific activity can be improved by increasing the amount of ^{18}F-SFB in the radiolabelling reaction. However increasing the ratio of ^{18}F-SFB to scFv in the radiolabeling reaction also causes an increased loss of scFv binding activity. A 5 fold increase in the ratio of ^{18}F-SFB to scFv increases the specific activity by 3.5 fold (data not shown), but also causes a reduction in $scFv_{anti\text{-}LIBS}$ binding to activated platelets in flow cytometry to 2% of positive staining (data not shown) in comparison to non-labeled $scFv_{anti\text{-}LIBS}$ with 62% of platelets positive. Several optimization reactions were conducted at the outset to determine the optimal ratio of ^{18}F-SFB to scFv used in this study to balance specific activity and immunoreactivity. We felt that a lowered specific activity was more acceptable than a large loss of antibody activity.

VOI analysis in animals injected with the targeted scFv show the ratio of SUV_{max} of the injured vessel : skeletal muscle being significantly higher than the SUV_{max} of the intact vessel : skeletal muscle for the duration of the PET scan. Subsequent immunohistochemistry of both the injured and intact vessels reveals that platelets and thrombi are only present in injured carotid arteries. Together these results are convincing evidence that the targeted scFv accumulates at the intended target: the carotid artery thrombus. This demonstrates ^{18}F-$scFv_{anti\text{-}LIBS}$ specific imaging of activated GPIIb/IIIa present in activated platelets which are a

component of the carotid artery thrombus. Imaging these small radiolabeled antibodies may be useful in the future to identify and quantify atherosclerotic plaques that are prone to thrombosis. In contrast the results of the biodistribution study shows that the radioactivity uptake in the injured vessel is only higher than the intact vessel in the earlier time point investigated. A possible explanation for this observation is that due to these tissues being extremely small, measuring the weight accurately is difficult and this may have affected the outcome of this measurement. In comparison, other recent immuno-PET studies [12] are designed to accumulate radiolabeled antibodies in tumor xenografts, these target tissues are orders of magnitude larger than the mouse carotid arteries investigated in this study. Another explanation for this observation may be the rapid clearance of scFvs from the blood pool: the level is high at 5 minutes post injection (10.5 ± 4.4 % ID/g) whilst at all other time points investigated, blood pool is very low (15 minutes: 6.3 ± 3.2 % ID/g, 30 minutes : 2.8 ± 0.8 % ID/g, 45 minutes: 3.9 ± 1.5 % ID/g). The thrombus in the injured vessel will still continue to break apart (loss of radioactivity) and build up with new activated platelets (increase in radioactivity uptake). However, after 5 minutes there is much less circulating ^{18}F-scFv$_{\text{anti-LIBS}}$ and as a result, less radioactivity is now incorporated into the thrombus. At the same time previously bound ^{18}F-scFv$_{\text{anti-LIBS}}$ on activated platelets is breaking off in fragments from the wall adherent thrombus in the injured vessel and is being cleared from circulation. So previously bound ^{18}F-scFv$_{\text{anti-LIBS}}$ on these fragments gets cleared from the system and are not available in circulation to re-bind to the thrombus. Blood pool of ^{18}F-scFv$_{\text{anti-LIBS}}$ is low at 5 minutes post injection, but is comparable to previous studies using scFvs radiolabeled with ^{124}Iodine for tumor imaging [40]. Clearance of thrombus fragments and activated platelets bound to ^{18}F-scFv$_{\text{anti-LIBS}}$ in circulation may also be a reason why we see a relatively low blood pool at 5 minutes.

PET is an attractive technique that has previously been studied as a method to detect vulnerable atherosclerotic plaques. Others have used non-targeted ^{18}FDG in clinical studies as a method to quantify inflammation associated with rupture prone plaques [41]. One drawback to this approach is that inflammation is not a process specific to atherosclerosis, and ^{18}FDG has significant background uptake in unrelated tissues with high energy requirement such as the brain or the heart. Detection of molecular markers that are specifically expressed in atherosclerotic plaques would avoid the problems of high background in unrelated tissues. Small peptides that bind to VCAM-1 expressed in activated or damaged endothelial cells have been investigated as a potential method of detection and quantification of vulnerable atherosclerotic plaques [42]. This study demonstrated good specific uptake of their ^{18}F-labeled peptide in atherosclerotic vessels of ApoE$^{-/-}$ KO mice fed a high fat diet. VCAM-1 expression is associated with the early stage of lesion development in atherosclerosis [43,44]. Activated platelets are not only recruited to the injured endothelium in early lesion development, but they are also associated with the thrombus that forms when the lesion undergoes minor rupture events [4,45]. This feature of activated platelets suggests that ^{18}F-scFv$_{\text{anti-LIBS}}$ would be a useful radiotracer to detect and quantify atherosclerosis in both the early stage of lesion development and in the later stage of disease where the plaque is undergoing repeated rupture and repair [46]. This will be investigated in future studies. The $FeCl_3$ induced vascular thrombosis is one of the most commonly used models of vascular thrombosis [47,48]. Complete vessel occlusion can be achieved within 20 minutes using solutions of $FeCl_3$ 10 % or greater [49]. Decreasing the concentration of $FeCl_3$, as we have done in this study, produces a vessel-wall-adherent non-occlusive thrombus that mimics what is seen in the development of human lesions, where activated platelets accumulate on the surface of a plaque. Therefore, this animal model of vascular thrombosis resembles the

clinical situation of the growing atherosclerotic lesion in humans, which continually draws activated platelets during its buildup.

Conclusions

This study demonstrates the rapid accumulation of ^{18}F-scFv$_{anti\text{-}LIBS}$ in thrombi containing platelets expressing GPIIb/IIIa in the active conformation. PET sensitivity is several orders of magnitude higher than other imaging modalities and is especially relevant for the detection of molecular markers that are only present in minute amounts. Our radiotracer can potentially be used to detect areas in vessels that are at risk of imminent plaque rupture. In particular this will allow monitoring of vessels in “danger” areas such as coronary arteries and carotid arteries, where a thrombus can cause a blockage that may prove to be fatal. This will be investigated in future studies.

Acknowledgments

This work was funded by the National Health and Medical Research Council (NHMRC), Grants 1029249, 1017670 and 1011418. K.Ar. is supported by the NHMRC and the National Heart Foundation (586740). K.Al. is supported by the German Research Foundation (AL 1521/1-1). K.P. is supported by an Australian Research Council Future Fellowship (FT0992210). C.E.H. is supported by a NHMRC Fellowship (472668). The work was also supported in part by the Victorian Government’s Operational Infrastructure Support Program.

References

[1] Varnava AM, Mills PG, Davies MJ. Relationship between coronary artery remodeling and plaque vulnerability. Circulation 2002;105:939–43.

[2] Schafer A, Bauersachs J. Endothelial dysfunction, impaired endogenous platelet inhibition and platelet activation in diabetes and atherosclerosis. Curr Vasc Pharmacol 2008;6:52–60.

[3] Hansson GK. Inflammation, atherosclerosis, and coronary artery disease. N Engl J Med 2005;352:1685–95.

[4] Gawaz M, Langer H, May AE. Platelets in inflammation and atherogenesis. J Clin Invest 2005;115:3378–84.

[5] Gawaz M, Stellos K, Langer HF. Platelets modulate atherogenesis and progression of atherosclerotic plaques via interaction with progenitor and dendritic cells. J Thromb Haemost 2008;6:235–42.

[6] von zur Muhlen C, von Elverfeldt D, Moeller JA, Choudhury RP, Paul D, Hagemeyer CE, et al. Magnetic resonance imaging contrast agent targeted toward activated platelets allows in vivo detection of thrombosis and monitoring of thrombolysis. Circulation 2008;118:258–67.

[7] von Elverfeldt D, von zur Muhlen C, Wiens K, Neudorfer I, Zirlik A, Meißner M, et al. In vivo detection of activated platelets allows characterizing rupture of atherosclerotic plaques with molecular magnetic resonance imaging in mice. PLoS One 2012;7:e45008.

[8] Choudhury RP, Fuster V, Fayad ZA. Molecular, cellular and functional imaging of atherothrombosis. Nat Rev Drug Discov 2004;3:913–25.

[9] Choudhury RP, Fisher EA. Molecular imaging in atherosclerosis, thrombosis, and

vascular inflammation. Arterioscler Thromb Vasc Biol 2009;29:983–91.

[10] Nahrendorf M, Jaffer FA, Kelly KA, Sosnovik DE, Aikawa E, Libby P, et al. Noninvasive vascular cell adhesion molecule-1 imaging identifies inflammatory activation of cells in atherosclerosis. Circulation 2006;114:1504–11.

[11] Spuentrup E, Buecker A, Katoh M, Wiethoff AJ, Parsons EC, Botnar RM, et al. Molecular magnetic resonance imaging of coronary thrombosis and pulmonary emboli with a novel fibrin-targeted contrast agent. Circulation 2005;111:1377–82.

[12] Wu AM. Antibodies and antimatter: the resurgence of immuno-PET. J Nucl Med 2009;50:2–5.

[13] Bell A, Wang ZJ, Arbabi-Ghahroudi M, Chang TA, Durocher Y, Trojahn U, et al. Differential tumor-targeting abilities of three single-domain antibody formats. Cancer Lett 2010;289:81–90.

[14] Holliger P, Hudson PJ. Engineered antibody fragments and the rise of single domains. Nat Biotechnol 2005;23:1126–36.

[15] Hagemeyer CE, zur Muhlen von C, Elverfeldt von D, Peter K. Single-chain antibodies as diagnostic tools and therapeutic agents. Thromb Haemost 2009;101:1012–9.

[16] von zur Muhlen C, Sibson NR, Peter K, Campbell SJ, Wilainam P, Grau GE, et al. A contrast agent recognizing activated platelets reveals murine cerebral malaria pathology undetectable by conventional MRI. J Clin Invest 2008;118:1198–207.

[17] von zur Muhlen C, Peter K, Ali ZA, Schneider JE, McAteer MA, Neubauer S, et al. Visualization of activated platelets by targeted magnetic resonance imaging utilizing conformation-specific antibodies against glycoprotein IIb/IIIa. J Vasc Res 2009;46:6–14.

[18] McAteer MA, Akhtar AM, von zur Muhlen C, Choudhury RP. An approach to molecular

imaging of atherosclerosis, thrombosis, and vascular inflammation using microparticles of iron oxide. Atherosclerosis 2010;209:18–27.

[19] Sureshbabu W, Mawlawi O. PET/CT imaging artifacts. J Nucl Med Technol 2005;33:156–61.

[20] Rudd JHF, Fayad ZA. Imaging atherosclerotic plaque inflammation. Nat Clin Pract Cardiovasc Med 2008;5:S11–7.

[21] Sinusas AJ, Bengel F, Nahrendorf M, Epstein FH, Wu JC, Villanueva FS, et al. Multimodality cardiovascular molecular imaging, part I. Circ Cardiovasc Imaging 2008;1:244–56.

[22] Heidt T, Deininger F, Peter K, Goldschmidt J, Pethe A, Hagemeyer CE, et al. Activated platelets in carotid artery thrombosis in mice can be selectively targeted with a radiolabeled single-chain antibody. PLoS One 2011;6:e18446.

[23] Stoll P, Bassler N, Hagemeyer CE, Eisenhardt SU, Chen YC, Schmidt R, et al. Targeting ligand-induced binding sites on GPIIb/IIIa via single-chain antibody allows effective anticoagulation without bleeding time prolongation. Arterioscler Thromb Vasc Biol 2007;27:1206–12.

[24] Wang X, Hagemeyer CE, Hohmann JD, Leitner E, Armstrong PC, Jia F, et al. Novel single-chain antibody-targeted microbubbles for molecular ultrasound imaging of thrombosis: validation of a unique noninvasive method for rapid and sensitive detection of thrombi and monitoring of success or failure of thrombolysis in mice. Circulation 2012;125:3117–26.

[25] Ta HT, Prabhu S, Leitner E, Jia F, Elverfeldt von D, Jackson KE, et al. Enzymatic single-chain antibody tagging: a universal approach to targeted molecular imaging and cell homing in cardiovascular disease. Circ Res 2011;109:365–73.

[26] Schwarz M, Katagiri Y, Kotani M, Bassler N, Loeffler C, Bode C, et al. Reversibility versus persistence of GPIIb/IIIa blocker-induced conformational change of GPIIb/IIIa ($\alpha_{IIb}\beta_3$, CD41/CD61). J Pharmacol Exp Ther 2004;308:1002–11.

[27] Vaidyanathan G, Zalutsky MR. Synthesis of N-succinimidyl 4-[^{18}F]fluorobenzoate, an agent for labeling proteins and peptides with ^{18}F. Nat Protoc 2006;1:1655–61.

[28] von zur Muhlen C, von Elverfeldt D, Choudhury RP, Ender J, Ahrens I, Schwarz M, et al. Functionalized magnetic resonance contrast agent selectively binds to glycoprotein IIb/IIIa on activated human platelets under flow conditions and is detectable at clinically relevant field strengths. Mol Imaging 2008;7:59–67.

[29] Ackermann U, Yeoh SD, Sachinidis JI, Poniger SS, Scott AM, Tochon Danguy HJ. A simplified protocol for the automated production of succinimidyl 4−[^{18}F] fluorobenzoate on an IBA Synthera module. J Labelled Comp Radiopharm 2011;54:671–3.

[30] Wagner CL, Mascelli MA, Neblock DS, Weisman HF, Coller BS, Jordan RE. Analysis of GPIIb/IIIa receptor number by quantification of 7E3 binding to human platelets. Blood 1996;88:907–14.

[31] Hagemeyer CE, Peter K. Targeting the platelet integrin GPIIb/IIIa. Curr Pharm Des 2010;16:4119–33.

[32] Smyth SS, Tsakiris DA, Scudder LE, Coller BS. Structure and function of murine alphaIIbbeta3 (GPIIb/IIIa): studies using monoclonal antibodies and beta3-null mice. Thromb Haemost 2000;84:1103–8.

[33] Marx RE. Platelet-rich plasma: evidence to support its use. J Oral Maxillofac Surg 2004;62:489–96.

[34] Cai W, Olafsen T, Zhang X, Cao Q, Gambhir SS, Williams LE, et al. PET imaging of

colorectal cancer in xenograft-bearing mice by use of an ^{18}F-labeled T84.66 anti-carcinoembryonic antigen diabody. J Nucl Med 2007;48:304–10.

[35] Langer HF, Haubner R, Pichler BJ, Gawaz M. Radionuclide imaging: a molecular key to the atherosclerotic plaque. J Am Coll Cardiol 2008;52:1–12.

[36] Laitinen I, Saraste A, Weidl E, Poethko T, Weber AW, Nekolla SG, et al. Evaluation of alphavbeta3 integrin-targeted positron emission tomography tracer ^{18}F-galacto-RGD for imaging of vascular inflammation in atherosclerotic mice. Circ Cardiovasc Imaging 2009;2:331–8.

[37] Bassler N, Loeffler C, Mangin P, Yuan Y, Schwarz M, Hagemeyer CE, et al. A mechanistic model for paradoxical platelet activation by ligand-mimetic alphaIIb beta3 (GPIIb/IIIa) antagonists. Arterioscler Thromb Vasc Biol 2007;27:e9–15.

[38] Du XPX, Plow EFE, Frelinger ALA, O'Toole TET, Loftus JCJ, Ginsberg MHM. Ligands “activate” integrin alpha IIb beta 3 (platelet GPIIb-IIIa). Cell 1991;65:409–16.

[39] Kenanova V, Wu AM. Tailoring antibodies for radionuclide delivery. Expert Opin Drug Deliv 2006;3:53–70.

[40] Olafsen T, Wu AM. Antibody vectors for imaging. Semin Nucl Med 2010;40:167–81.

[41] Rudd JHF, Warburton EA, Fryer TD, Jones HA, Clark JC, Antoun N, et al. Imaging atherosclerotic plaque inflammation with [^{18}F]-fluorodeoxyglucose positron emission tomography. Circulation 2002;105:2708–11.

[42] Nahrendorf M, Keliher E, Panizzi P, Zhang H, Hembrador S, Figueiredo JL, et al. ^{18}F-4V for PET-CT imaging of VCAM-1 expression in atherosclerosis. JACC Cardiovasc Imaging 2009;2:1213–22.

[43] Jaffer FA, Libby P, Weissleder R. Optical and multimodality molecular imaging: insights into atherosclerosis. Arterioscler Thromb Vasc Biol 2009;29:1017–24.

[44] Libby P. Inflammation in atherosclerosis. Nature 2002;420:868–74.

[45] Jennings LK. Role of platelets in atherothrombosis. Am J Cardiol 2009;103:4–10.

[46] Thim T, Hagensen MK, Bentzon JF, Falk E. From vulnerable plaque to atherothrombosis. J Intern Med 2008;263:506–16.

[47] Woollard KJ, Sturgeon S, Chin-Dusting JPF, Salem HH, Jackson SP. Erythrocyte hemolysis and hemoglobin oxidation promote ferric chloride-induced vascular injury. J Biol Chem 2009;284:13110–8.

[48] Owens AP, Lu Y, Whinna HC, Gachet C, Fay WP, Mackman N. Towards a standardization of the murine ferric chloride-induced carotid arterial thrombosis model. J Thromb Haemost 2011;9:1862–3.

[49] Day SM, Reeve JL, Myers DD, Fay WP. Murine thrombosis models. Thromb Haemost 2004;92:486–94.

Figure legends

Figure 1: Flow cytometry comparing binding of non-labeled scFvs and radiolabeled scFvs

The purple filled curve represents antibody binding to non-activated platelets and the green curve shows binding to activated platelets. Fig. 1A shows a lower fluorescence signal when platelets are incubated with radiolabeled $scFv_{anti\text{-}LIBS}$ (right) compared to the non-labeled $scFv_{anti\text{-}LIBS}$ (left), indicating the labeled scFv has diminished binding activity in comparison to the same non-labeled scFv (n=7). Fig. 1B shows no binding of the mut-scFv regardless of radiolabeling.

Figure 2: Assessment of radiolabeled scFv binding to in vitro formed platelet rich clots

Clots incubated with the targeted $scFv_{anti\text{-}LIBS}$ showed significantly higher amounts of retained activity bound to the clot in comparison to clots incubated with non-targeted mut-scFv (Fig. 2A, n=9). After incubation with the radiolabeled scFvs, clots were frozen in OCT and sectioned at 7µm thickness and stained using the human anti-platelet marker CD41. All *in vitro* clots were positive for CD41, demonstrating the presence of platelets. The omit primary control staining showed no signal (Fig. 2B). Pre-incubation with cold $scFv_{anti\text{-}LIBS}$ results in a dose depended reduction of tracer binding, indicating specific interaction between the radio-tracer and the platelet integrin (Fig. 2C, n=3).

Figure 3: Biodistribution of radiolabeled $scFv_{anti\text{-}LIBS}$

Radioactivity uptake in the different organs was measured using a gamma counter and expressed as percentage injected dose per gram of tissue. Specific enrichment of targeted $scFv_{anti\text{-}LIBS}$ in the injured vessel is shown. Clearance from the blood and rapid elimination via the kidney is demonstrated (Fig. 3A, n=6). A strong reduction in the *in vivo* uptake of ^{18}F-

$scFv_{anti\text{-}LIBS}$ at the 5 minute biodistribution time point is observed with the pre injection of cold, non-labeled $scFv_{anti\text{-}LIBS}$. This indicates specific interaction between the radio-tracer and the platelet integrin (Fig. 3B, n=3).

Figure 4: Co registered PET/CT image of a mouse injected with targeted $scFv_{anti\text{-}LIBS}$

Uptake of ^{18}F-$scFv_{anti\text{-}LIBS}$ in the target area of $FeCl_3$ injury (arrow) is shown in transverse, sagital and coronal PET/CT views 45 min after injection (Fig. 4A). Other areas of high tracer uptake are the kidneys and the bladder. After PET scanning both carotid arteries from the mice were collected and frozen in OCT for histology. 7 µm sections from both the injured vessel and the intact vessel were stained for the mouse CD41 platelet marker. Positive (vector red) staining for platelets is observed in the injured vessel and is absent in the intact vessel sections (Fig. 4B).

Figure 5: PET image analysis

Image analysis shows higher specific uptake in the injured vessel when mice are injected with ^{18}F-$scFv_{anti\text{-}LIBS}$ (blue line, Fig. 5A, n=8) compared to mice injected with the non-targeted mut-scFv (red line, Fig. 5A, n=8). This specific difference is also evident when comparing the ratio between injured to intact vessel for ^{18}F-$scFv_{anti\text{-}LIBS}$ (blue line, Fig. 5B, n=8) and there is no difference for the non-targeted mut-scFv (red line, Fig. 5B, n=8). Fig 5C shows the CT image of a mouse with VOI's generated over the injured vessel in aqua and a VOI over the skeletal muscle with the equivalent volume.

Figure 1

Click here to download high resolution image

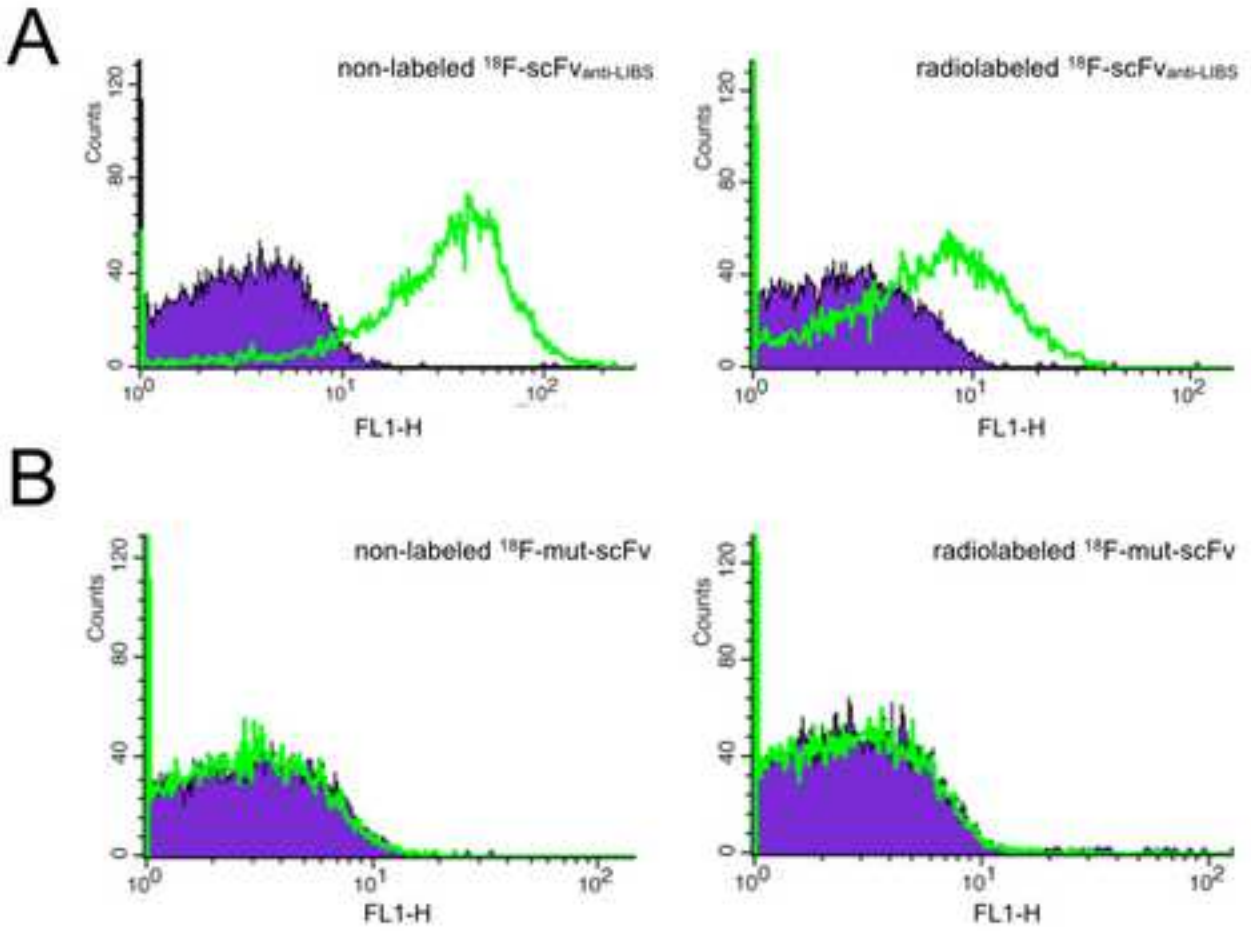


Figure 2

Click here to download high resolution image

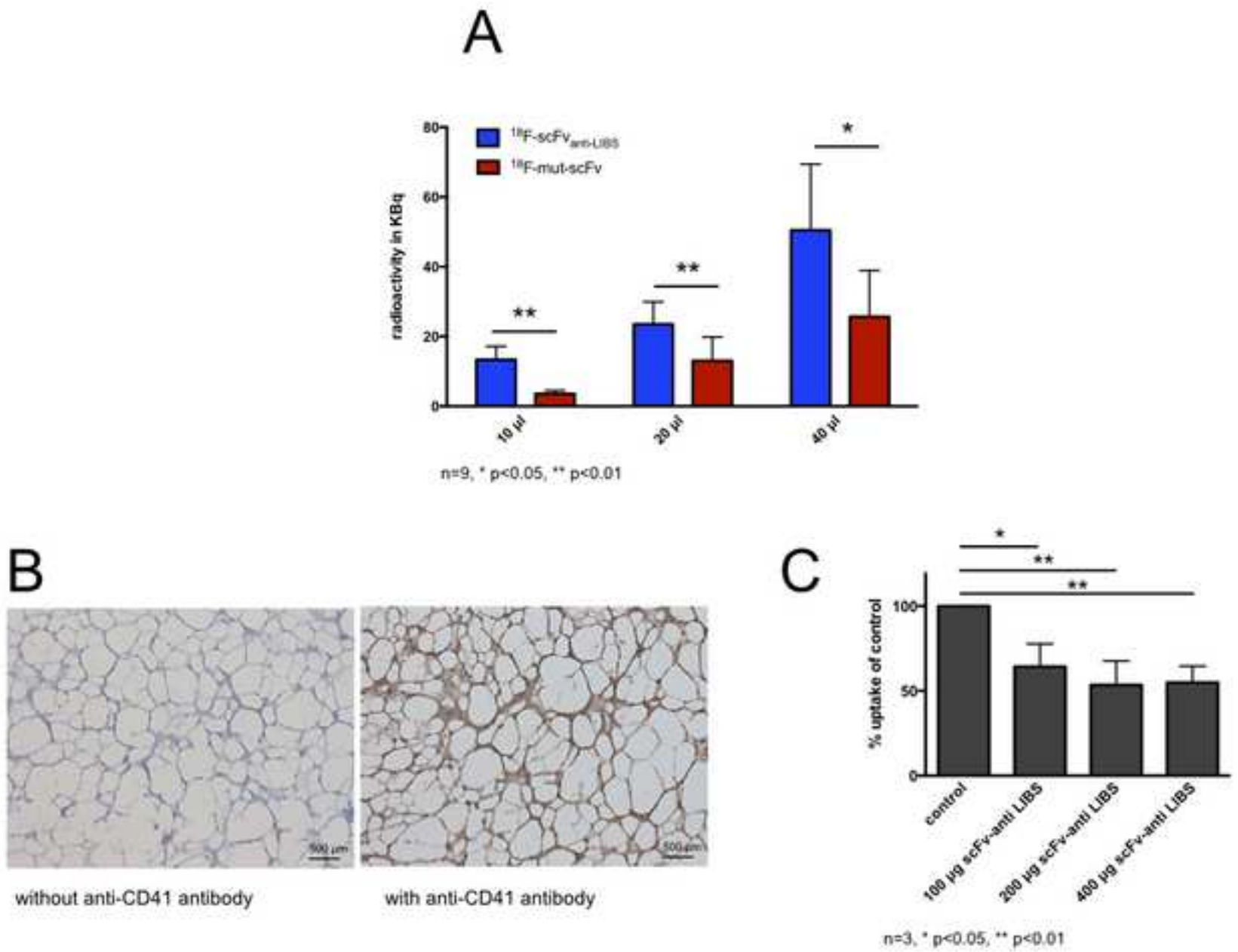


Figure 3

Click here to download high resolution image

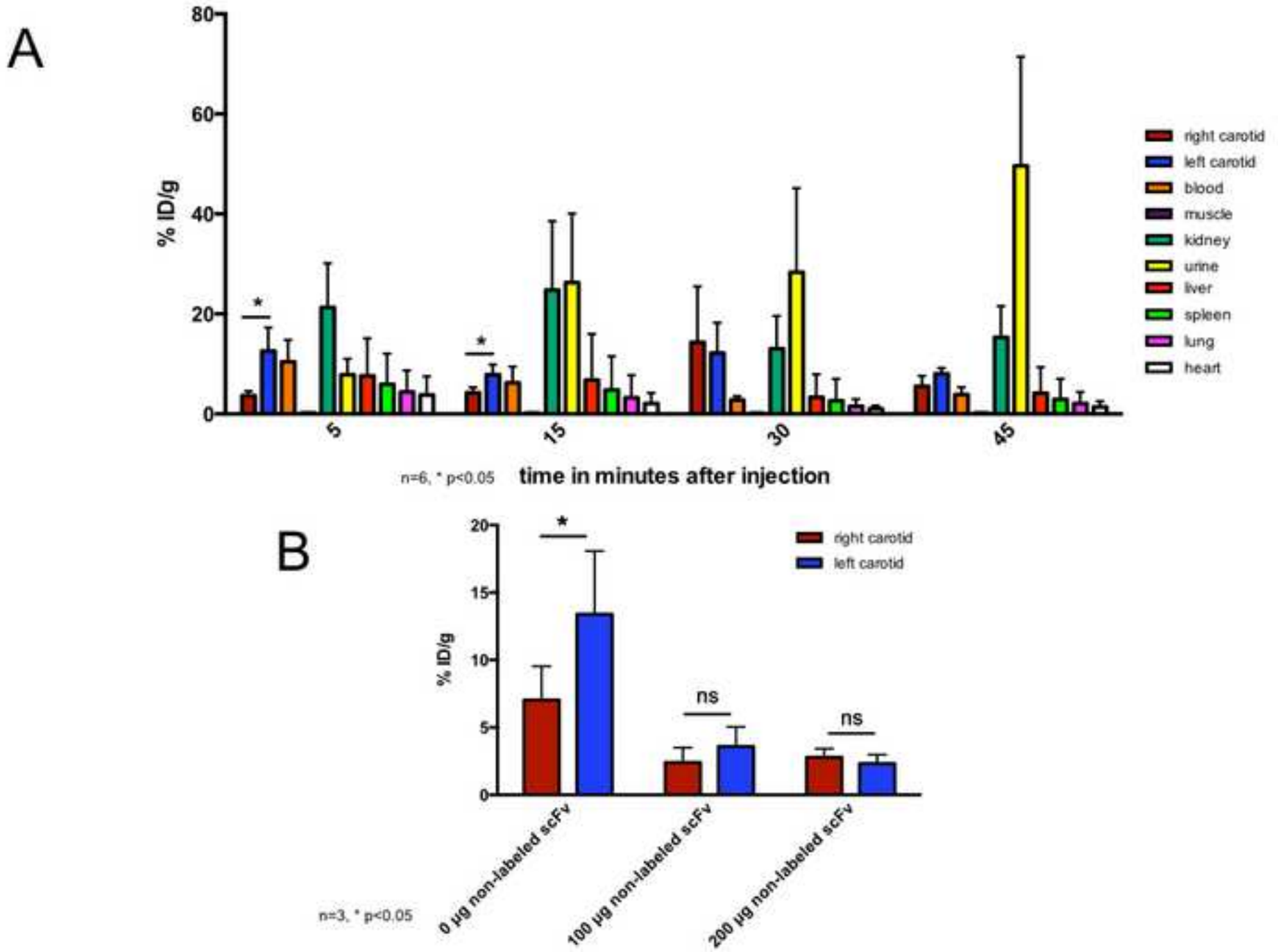


Figure 4

Click here to download high resolution image

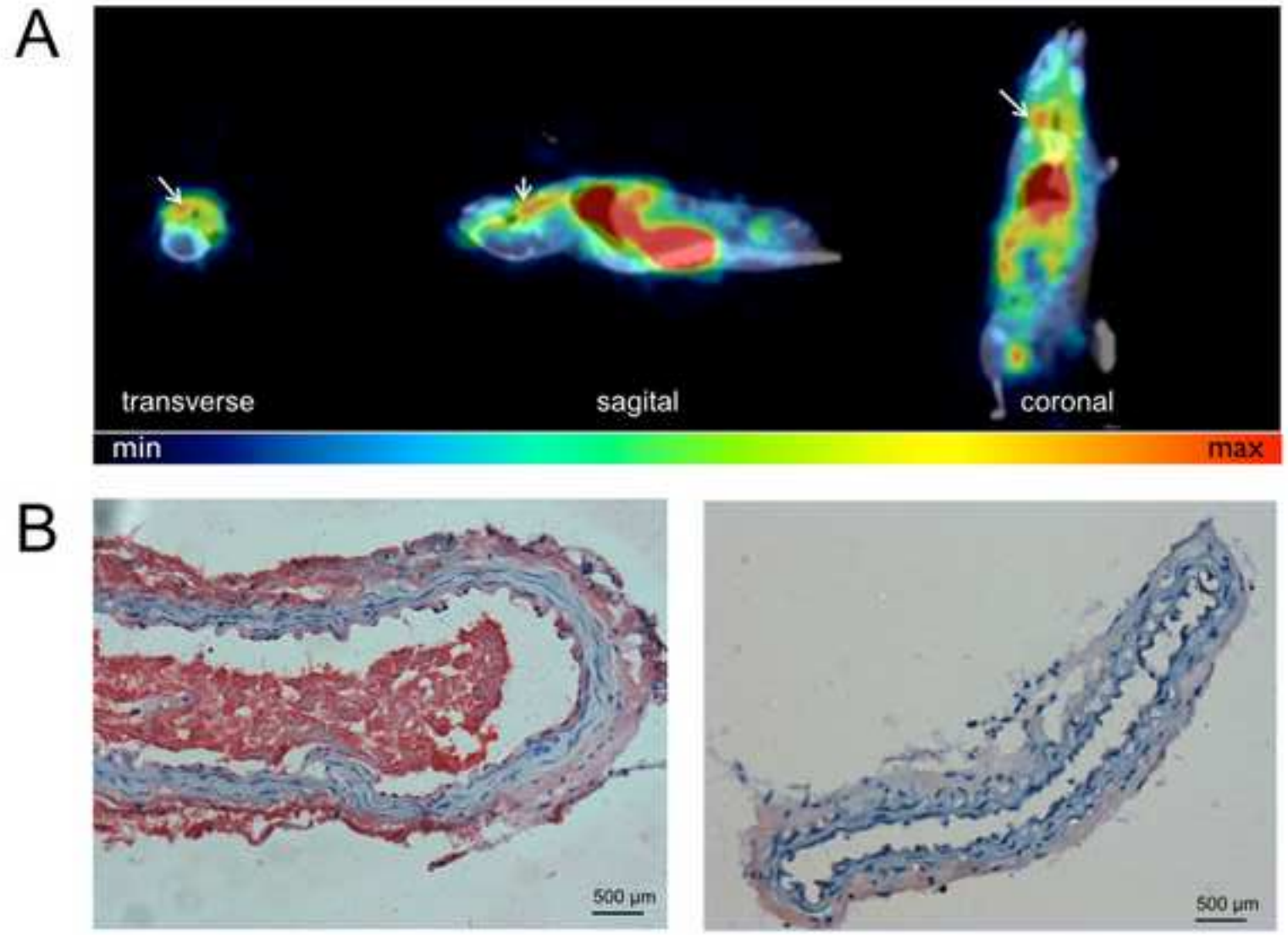


Figure 5
Click here to download high resolution image

